

## OH EMISSION AND THE NATURE OF MINKOWSKI'S FOOTPRINT (M1–92)

E. R. SEAQUIST AND RENÉ PLUME<sup>1</sup>  
Department of Astronomy, University of Toronto

AND

L. E. DAVIS  
National Optical Astronomy Observatories, Tucson, Arizona*Received 1990 March 14; accepted 1990 July 23*

## ABSTRACT

We present VLA observations of the 1667 and 1612 MHz OH brightness distribution in the bipolar nebula M1–92. The OH emission originates in the circumstellar gas disk whose axis coincides with that of the bipolar lobes. No OH emission is found in the lobes themselves. A simple axisymmetric model which describes the main features of this emission consists of a fan-shaped disk undergoing pure radial expansion at a velocity of  $18 \text{ km s}^{-1}$ . In this model, the radius of the disk is  $2''.4$  ( $1.6 \times 10^{17} \text{ cm}$ ) and the opening angle of the fan is  $70^\circ$  (FWHM). The bipolar axis is inclined at  $35^\circ$  to the line of sight. The mass-loss rate in the disk is estimated to be  $5.6 \times 10^{-6} M_\odot \text{ yr}^{-1}$  for an assumed distance of 4.5 kpc, and the kinematic age of the disk is  $\sim 3000 \text{ yr}$ .

The properties of M1–92 are reviewed, including the mass-loss rate, the kinematic age, the IR characteristics, and the radio continuum emission, and all are found to be consistent with the view that M1–92 is a young planetary nebula.

*Subject headings:* interstellar: molecules — nebulae: individual (M1–92) — nebulae: internal motions

## I. INTRODUCTION

The object M1–92 (Minkowski's footprint) is a bipolar nebula originally discovered by Minkowski (1946). It is similar to a number of other bipolar nebulae, including CRL 618, CRL 2688, OH 231.8 + 4.2 (= OH 9739), M3–99, and Parsamyan 21. The optical characteristics of M1–92 have been described in detail by Herbig (1975) and by Cohen and Kuhl (1977). Optically, it resembles a human footprint oriented in the sky with a position angle of  $131^\circ$ . The northwestern lobe forms the "sole" of the foot and is the larger and brighter of the two nebulosities. The smaller and fainter southeastern lobe forms the "heel." The two lobes are enclosed in an elliptical area with dimensions of  $4''.5 \times 11''.5$  and are separated by a gap (the "arch") of about  $2''$ . At the maximum estimated distance of 4.5 kpc (Herbig 1975), the corresponding linear dimensions projected on the sky would be  $3.0 \times 10^{17} \times 7.7 \times 10^{17} \text{ cm}$  with a gap size of  $1.3 \times 10^{17} \text{ cm}$ . Both Minkowski and Herbig interpreted the lobes as reflection nebulae with the gap arising from a dense circumstellar disk set at an angle to the line of sight, thereby obscuring the light from the southeastern lobe. Davis, Seaquist, and Purton (1979) estimated that the inclination of the disk axis to the line of sight is  $\sim 35^\circ$ .

Herbig (1975) concluded from an extrapolation of the colors of the lobes along the reddening line that the star at the center of the nebula is of type B0.5 V, essentially in agreement with a similar estimate (B1 V or B1 III) by Cohen and Kuhl (1977). However, since both lobes show reflected broad-lined P Cygni profiles with the absorption component blueshifted by  $530 \text{ km s}^{-1}$ , the star is the source of a fast wind. Such an outflow suggests that it is not an ordinary main-sequence star. The lobes also exhibit a sharp line emission spectrum of H, Fe II, [Fe II], Ti II, and Si I, giving velocities of  $-15 \text{ km s}^{-1}$  in the bright lobe and  $+17 \text{ km s}^{-1}$  in the faint lobe. These features

probably refer to conditions farther out in the nebula, where the outflow velocity is lower.

Bowers and Knapp (1989) detected continuum emission at 4885 MHz from M1–92. The angular extent of this emission is slightly larger than their beam ( $5''$ ), indicating that an extended region of the nebula is ionized by the central star. They note that the existence of this ionization is consistent with the classification of the central star.

Lepine and Nguyen-Quang-Rieu (1974) first detected OH emission in M1–92 at 1612 MHz and 1667 MHz, indicating the presence of molecular gas in the system. There appears to be little or no emission at 1665 MHz (Fix and Mutel 1977), and there appear not to be any published measurements at 1720 MHz. These detections were confirmed by Davis, Seaquist, and Purton (1979), who also showed that no changes were detected since the earlier measurements. Since then, this object has been found to be an IRAS source (IRAS 19343 + 2926), as well as a source of CO emission (Knapp 1986).

The evolutionary state of M1–92 has been somewhat controversial. Recent studies have shown that young stellar objects (YSO) exhibit many of the properties seen in M1–92. For example, high-velocity outflows are often associated with YSOs and many of these outflows show some degree of collimation (Lada 1985). Also, some bipolar outflows in star forming regions have been found to have dense, rotating, circumstellar disks much like that seen in M1–92 (Kaifu *et al.* 1984; Takano *et al.* 1984; Torrelles *et al.* 1986). These similarities, however, seem to be little more than superficial, and other observational evidence indicates that M1–92 is not a YSO but may be a young planetary nebula (PN) instead. Evidence against the YSO hypothesis comes from Eiroa *et al.* (1983), who state that the  $\text{H}_2\text{O}$  ice features found in the spectrum of M1–92 do not match those seen in molecular clouds. More specifically, comparison of the  $3.1 \mu\text{m}$   $\text{H}_2\text{O}$  ice absorption line of M1–92 with laboratory measurements of the absorption produced by crystalline and amorphous ice grains

<sup>1</sup> Currently at Department of Astronomy, University of Texas.

yields a better fit with the crystalline ice. In contrast, Leger *et al.* (1979) found that amorphous ice grains are a better fit to the ice absorption features of IR objects in molecular clouds. There is also the noteworthy point made by Herbig (1975) that M1–92 does not appear associated with any region of heavy interstellar obscuration as would be expected for a star forming region.

Expanding disks of the type seen in M1–92 are often found in PN. However, the temperature of the central star implied by its spectral class (27,000 K) is rather low for a full-fledged PN, since they are characterized by temperatures in excess of 50,000 K and up to 250,000 K (Abell 1966) and are located off the main sequence. If M1–92's central star is of spectral class B0.5 V, then its temperature and position on the H-R diagram place it far from the region of the PN nuclei. We note, however, that the position of such a star on the H-R diagram is near to the evolutionary track for a PN central star of approximately 0.8–1.0  $M_{\odot}$ . Most of these characteristics together with the radio detection by Bowers and Knapp (1989) suggest that M1–92 is an extremely young PN.

In this paper, we report VLA measurements of the OH line emission at 1667 MHz and 1612 MHz which show the structure of the disk region. We compare these results with a model for the 1667 MHz emission which provides a simple geometric framework for understanding the features of this object.

## II. OBSERVATIONS

Our 1667 MHz and 1612 MHz OH line observations of M1–92 were made with the Very Large Array (VLA)<sup>2</sup> in a 4 hr observing period on 1983 September 19. Twenty-four of the 27 antennas were used and set in the A-array configuration yielding an essentially circular synthesized beam of FWHM dimensions 1'06 at 1667 MHz and 1'41 × 1'05 at PA = –88°2 at 1612 MHz. All measurements were made in right circular polarization. The observations were made with 32 spectral line channels providing a channel separation of 12.207 kHz, equivalent to a velocity separation of 2.19 km s<sup>–1</sup> at 1667 MHz. The 1612 MHz observations employed a channel separation of 3.052 kHz, equivalent to a velocity separation of 0.57 km s<sup>–1</sup>. The source 1923+210 served as both a flux and a phase calibrator. The adopted flux of this source at both frequencies was 1.45 Jy as interpolated from observatory records for this source. No comparison was made with a primary calibrator such as 3C 286. We believe that the flux calibration is secure, however, since the measurements of the 1667 MHz line emission integrated over the source show excellent agreement with the single dish measurements of Davis, Seaquist, and Purton (1979) when allowance is made for the effects of the different velocity resolution. The total integration time on the source at 1667 MHz was 118 minutes, and the rms noise on the maps was found to be 6.5 mJy per channel, which is slightly higher than the theoretically predicted value of 5.3 mJy per channel. The integration time at 1612 MHz was 40 minutes, and the corresponding noise levels are 21 mJy per channel and 18.5 mJy per channel. Since there is no strong continuum emission associated with M1–92, no bandpass correction was applied to the data at either frequency.

We also report a brief search for continuum emission at 8440 MHz made on 1989 January 14, again in A-configuration. The

primary flux calibrator used was 3C 286 whose adopted flux density is 5.19 Jy. The bandwidth used was 100 MHz, and the total integration time was 14 minutes yielding a map rms of 0.03 mJy, which is consistent with the theoretical noise.

## III. RESULTS

### a) The 1667 MHz Emission

Figure 1 shows the individual OH line maps for channels 4–26. The remaining channels at each end of the spectrum do not show any signal. All maps were deconvolved using the CLEAN procedure and restored with a Gaussian beam of 1'07 × 1'06 at PA = –46°1. Figure 2 shows the spectrum of the integrated emission which compares favorably with previous single dish measurements, as noted previously. Figure 3 shows the data in the forms of a “zeroth moment” map (hereafter ZMM) representing the sum of all spectral line channels, and a “first moment” map (hereafter FMM) representing the distribution of the intensity-weighted mean velocity. These are shown together with respective maps representing the model to be discussed in the next section.

Figure 1 shows a change in the sign of the radial velocity of emission going from southeast (blueshifted) to northwest (redshifted) parallel to the axis of the bipolar lobes. This fact together with the bifurcation into two regions symmetrically placed about this axis indicates that the OH emission arises from a radially expanding disk or torus whose axis is tilted with respect to the line of sight, and whose orientation in the sky coincides with that of the bipolar nebula (PA = 131°). The sign of the OH velocity at each extreme is opposite to that found for the optical emission lines associated with the lobes which confirms that the OH emission is associated with the disk, and not the lobes. Figure 1 also shows that at the largest radial velocities are associated with features near the central star, and that the radial velocities tend to zero at large projected distance from the central star. The latter effect is similar to that detected in OH-IR stars and indicates the presence of emission from high-latitude regions. All of these features, including the radial expansion, the axis of symmetry, and the decrease in mean absolute radial velocity outward along this axis, are particularly evident in the FMM contours in Figure 3 and in the velocity profile in Figure 6. There is no evidence in any of these maps for detectable rotation of the disk. Later we develop a simple model to account for this structure.

A comparison of Figures 3a and c suggests that the star is positioned at the location of a shallow “hole” in the ZMM located at  $\alpha(1950) = 19^{\text{h}}34^{\text{m}}19^{\text{s}}.715$ ,  $\delta(1950) = 29^{\circ}26'04''.85$ . This conclusion is based on the coincidence between the “hole” and the axis of symmetry between the red and blue-shifted flows. If this is correct, then the star is not quite at the centroid of the ZMM which is at 19°683, 05'1. Figure 3c may be used to estimate the systemic velocity which appears to be about 4 km s<sup>–1</sup>. The ZMM in Figure 3a also yields an angular diameter for the masering region of about 5", measured perpendicular to the bipolar axis, corresponding to  $3.4 \times 10^{17}$  cm for a distance of 4.5 kpc.

Figure 1 shows a distinct similarity to channel maps of OH emission in the similar bipolar object OH 231.8+4.2 observed at similar resolution by Morris, Bowers, and Turner (1982). Both objects show evidence for an equatorial ring or disk. Some notable differences in OH 231.8+4.2 include the lack of an apparent deceleration toward the edge, the appearance of complete rings of emission in some individual channels, the

<sup>2</sup> The VLA is part of the National Radio Astronomy Observatory which is operated by Associated Universities, Inc., under a cooperative agreement with the National Science Foundation.

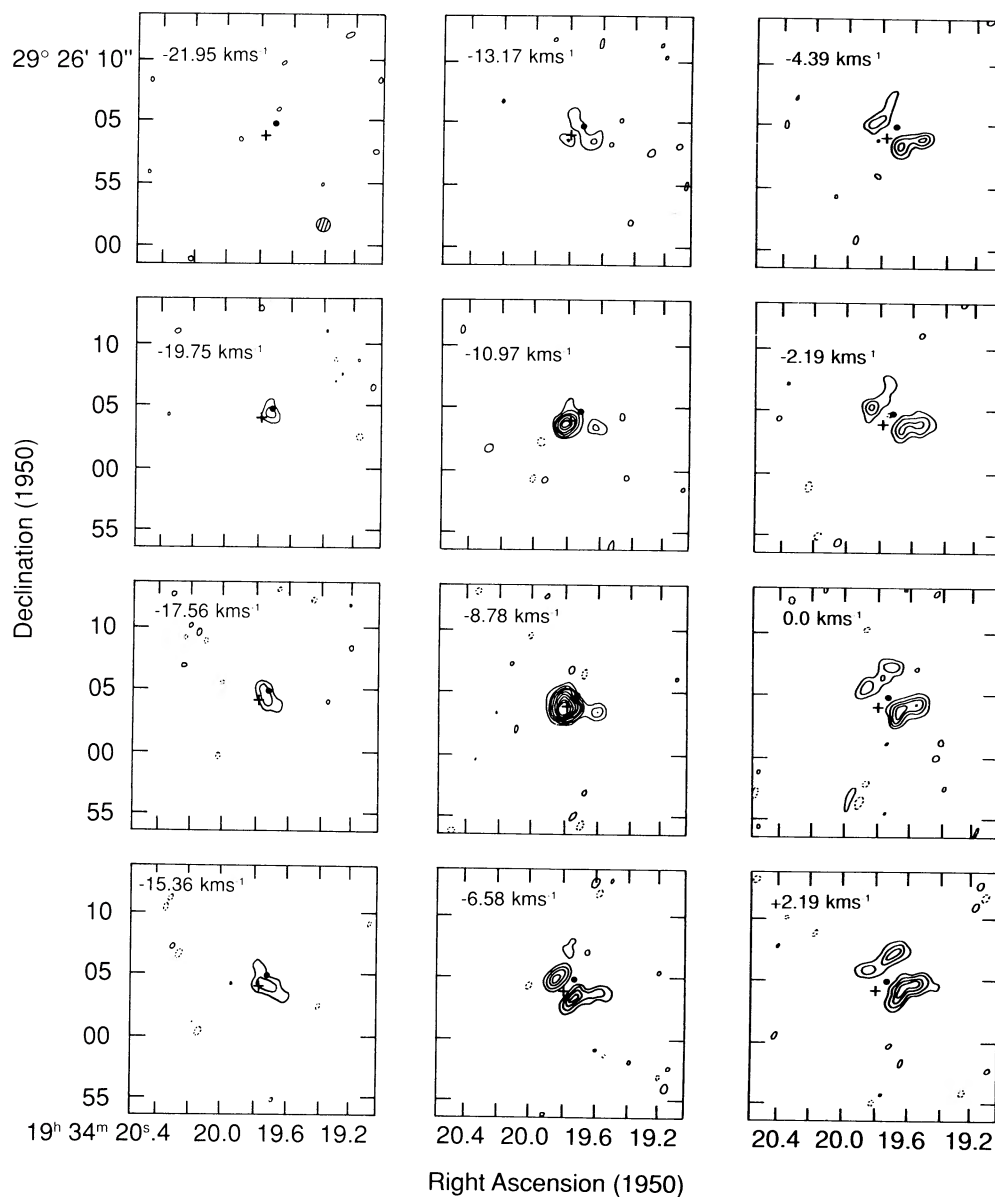


FIG. 1.—Channel maps of 1667 MHz OH Line. The last panel shows the stronger of the two channels showing the 1612 MHz line. The first contour and contour interval in all maps is  $0.18 \text{ Jy beam}^{-1}$ . The FWHM beam shape is shown at the bottom right of the first panel for the 1667 MHz line and in the last panel for the 1612 MHz line. The filled circle in each map shows the location of the minimum near the centroid of the zero moment map (Fig. 3a) which is assumed to be the position of the central star. The cross shows the position of the 1612 MHz emission.

evidence for OH emission originating within the bipolar reflection nebulae, and the occurrence of a “hotspot” in the center of the emission region. On the latter point, we note, however, that there are “hot spots” or emission peaks in M1–92 as described below, but they do not occur at the center.

An interesting feature of the M1–92 maps are the four emission peaks shown in Figure 3. The peaks are numbered increasing clockwise from the extreme southeastern feature. The spatial positions and velocities of these peaks indicate that they exist within the circumstellar disk itself and not the reflection lobes. Their orientation relative to the axis of the lobes suggests that their origin is related to the aspect and geometry of the disk rather than to random density enhancements. Two of the features (peaks 1 and 3) lie on the axis of the optical lobes, and the other two (peaks 2 and 4) lie on an orthogonal

axis. Peaks 1 and 3 coincide with exceptionally bright spots seen in the channel maps (Fig. 1) centered at  $V_{\text{LSR}} - 8.78 \text{ km s}^{-1}$  and  $6.58 \text{ km s}^{-1}$ , respectively. These are precisely the velocities of the intensity peaks in the integrated spectrum shown in Figure 2. In the spherical envelopes of OH–IR stars, these peaks coincide spatially with the stellar position. Presumably, the axisymmetric geometry in M1–92 is responsible, at least in part, for the displacements of these features along the symmetry axis. Peaks 2 and 4 are not as localized spatially or in velocity as 1 and 3. There is also an asymmetry in brightness between peaks 2 and 4 with peak 4 being the brighter of the two. The origin of these features will be discussed further in reference to our model in § IV. No continuum emission was detected at 1667 MHz, and the data allow a conservative upper limit of 20 mJy to be set.

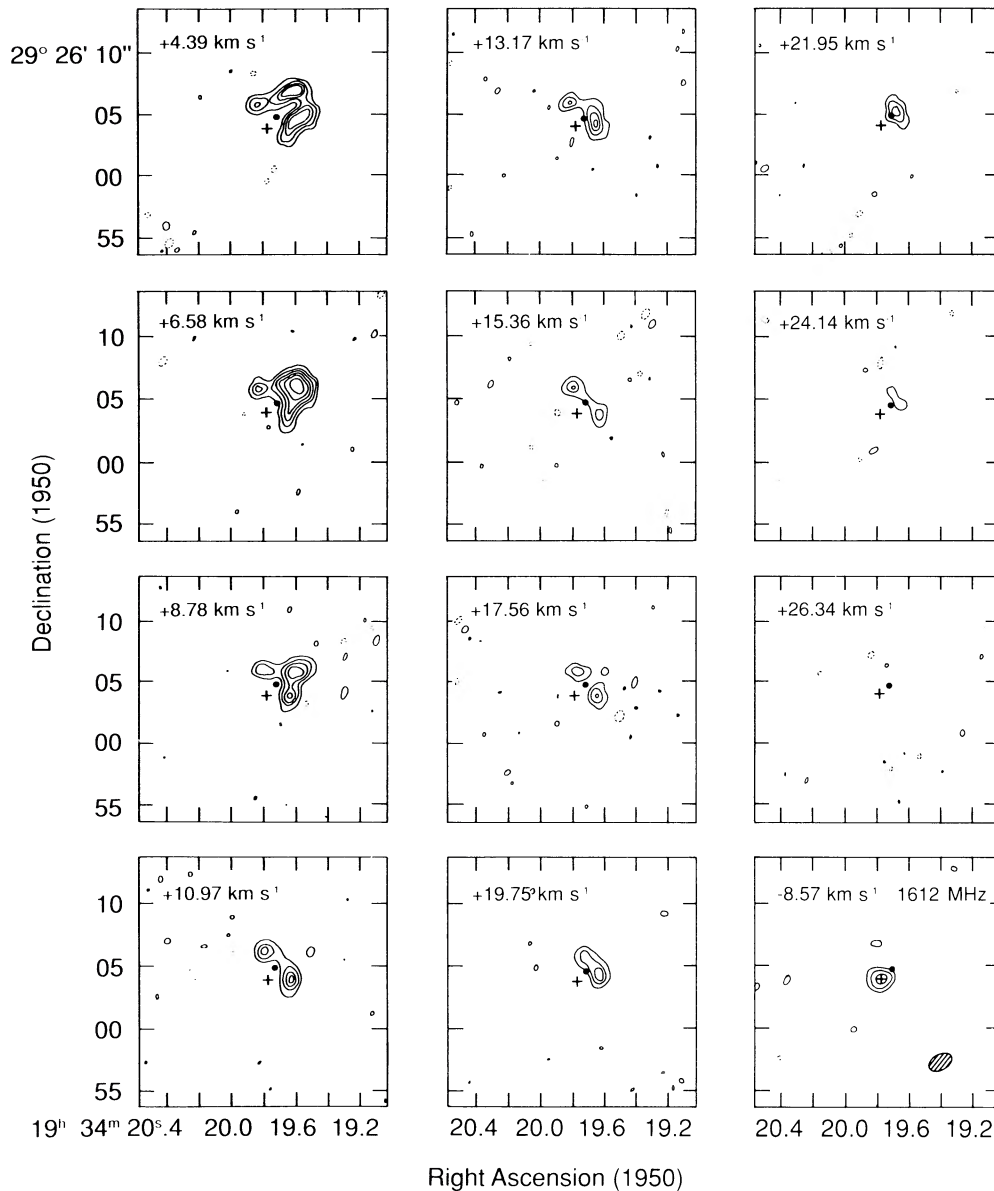


FIG. 1—Continued

#### b) The 1612 MHz Emission

The emission at 1612 MHz is weaker and is confined to two channels corresponding to  $V_{\text{LSR}} - 9.14 \text{ km s}^{-1}$  and  $-8.57 \text{ km s}^{-1}$ . This is consistent with our earlier observations reported in Davis, Seaquist, and Purton (1979). The emission in both channels is spatially unresolved and is located at 1950 coordinates  $\alpha = 19^{\text{h}}34^{\text{m}}19^{\text{s}}.774 \pm 0^{\text{s}}.007$ ,  $\delta = 29^{\circ}26'03''.95 \pm 0''.08$ . The distribution of the 1612 MHz emission in the stronger channel ( $V_{\text{LSR}} - 8.57 \text{ km s}^{-1}$ ) is shown in the last channel map in Figure 1. The location of the 1612 MHz emission spot is also marked with a cross on the 1667 MHz channel maps in Figure 1. The spot is essentially coincident in both velocity and position with peak 1 at 1667 MHz.

#### c) Continuum Emission at 8440 MHz

An unresolved ( $< 0''.3$ ) source with a flux of  $0.8 \pm 0.1 \text{ mJy}$  was found at 1950 coordinates  $\alpha = 19^{\text{h}}34^{\text{m}}19^{\text{s}}.22$ ,  $\delta =$

$29^{\circ}26'07''.5$ . This position is coincident with the peak of the lower resolution 4.9 GHz map made by Bowers and Knapp (1989) who found extended emission associated with M1-92. The extended emission is resolved out by our higher resolution observations. The unresolved resource is displaced  $5''.5$  to the northwest of the minimum in the OH emission, placing it well outside the OH emitting region and coincident with the northwestern bipolar lobe. No source stronger than  $0.1 \text{ mJy}$  was found within the OH emitting region itself.

#### IV. DISCUSSION

##### a) The Maser Pump

The maximum beam-averaged brightness temperature in the 1667 MHz OH emission is in peak 1 and corresponds to at least  $1.9 \times 10^5 \text{ K}$ , although a more typical value is about a factor of 5 lower ( $4 \times 10^4 \text{ K}$ ). Thus the emission is clearly nonthermal and we presume the source of emission is a maser.

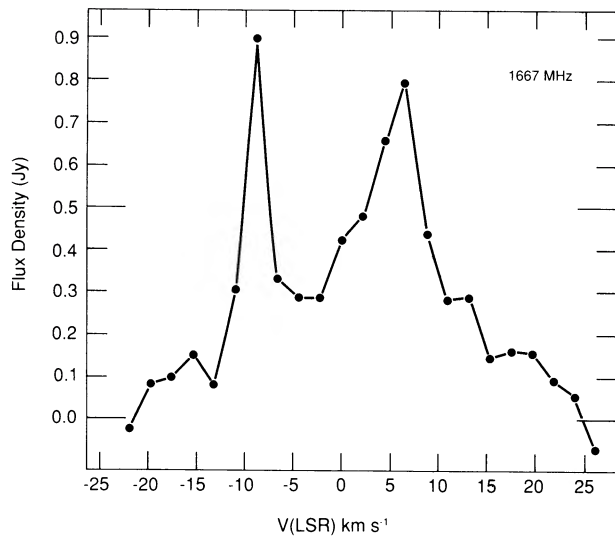


FIG. 2.—The spectrum of integrated flux densities found by integrating the channel maps.

This is probably the case at 1612 MHz as well. The pumping source is probably IR radiation. We have made a comparison of the number of microwave and continuum IR photons occupying the same velocity width as the maser. In the case of 1612 MHz emission, the pump photons may be either in the near-IR ( $2.8 \mu\text{m}$ ) or in the far-IR ( $35 \mu\text{m}$ ) (Elitzur, Goldreich, and Scoville 1976). The IR flux densities were found from interpolating

TABLE 1  
TABLE OF INFRARED FLUX DENSITIES FOR M1-92

Wavelength ( $\mu\text{m}$ )	Flux Density (Jy)	Reference
2.2.....	2.5	1
3.4.....	9.5	1
5.0.....	16.7	1
12.....	18	2
25.....	60	2
60.....	120	2
100.....	67	2

REFERENCES.—(1) Eiora *et al.* 1983; (2) IRAS Point Source Catalog 1988.

the IR data given in Table 1. The ratio of IR to microwave photons is about  $10^3$  at  $2.8 \mu\text{m}$  and  $10^4$  at  $35 \mu\text{m}$ . The 1667 MHz emission may be also pumped by far-IR (Elitzur 1978), and here the ratio is about  $10^2$  at  $35 \mu\text{m}$ . Thus, there would appear to be adequate IR emission available to pump the maser at both frequencies.

#### b) A Simple Geometric Model for the Maser in M1-92

We consider a simple model for the M1-92 equatorial disk containing the maser which explains many of the features observed. We assume throughout the discussion that the maser is saturated. This is supported qualitatively by the lack of evidence for variability. Figure 4 shows a schematic of the model. In this model, the disk is described in terms of a steady outflow

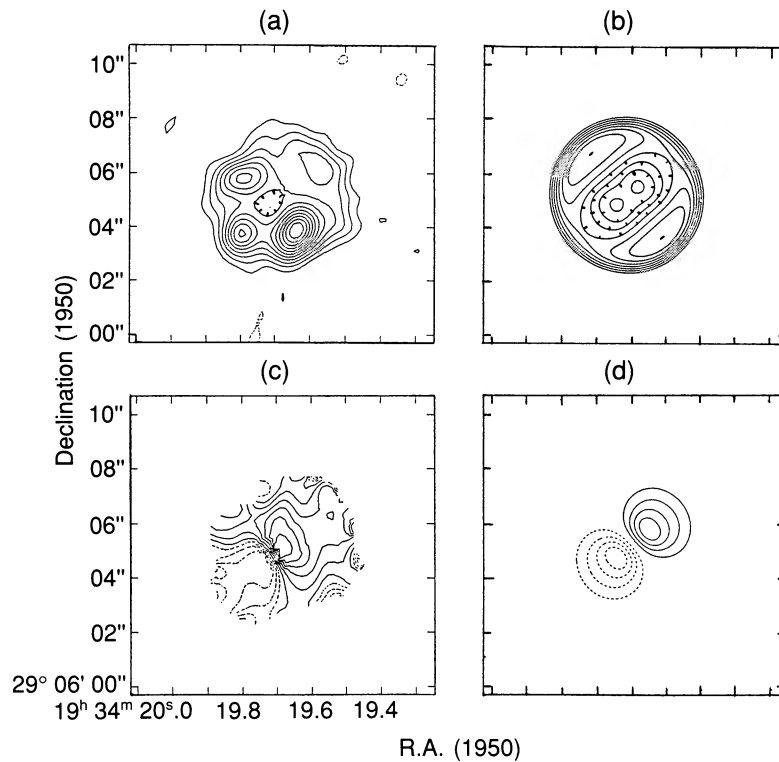


FIG. 3.—(a) Observed and (b) modeled contour maps of the zeroth moment of the 1667 MHz image cube. The contours in (a) are  $(-3, -2, -1, 1, 2, 3, 4, 5, 6, 7, 8, 9, 10, 11, 12) \times 0.0815 \text{ Jy km s}^{-1}$ . The contours in (b) are equal intervals in arbitrary units. The model map has been convolved with the circular Gaussian beam corresponding to that for the “CLEAN beam.” (c) Observed and (d) modeled contour maps of the first moment of the 1667 MHz image cube. The contours in (c) are  $(-15, -12, -9, -6, -3, 0, 3, 6, 9, 12, 15) \text{ km s}^{-1}$ . The contours in (d) are  $(-12, -9, -6, -3, 3, 6, 9, 12) \text{ km s}^{-1}$ . The model map has been convolved with the circular Gaussian “CLEAN beam.”

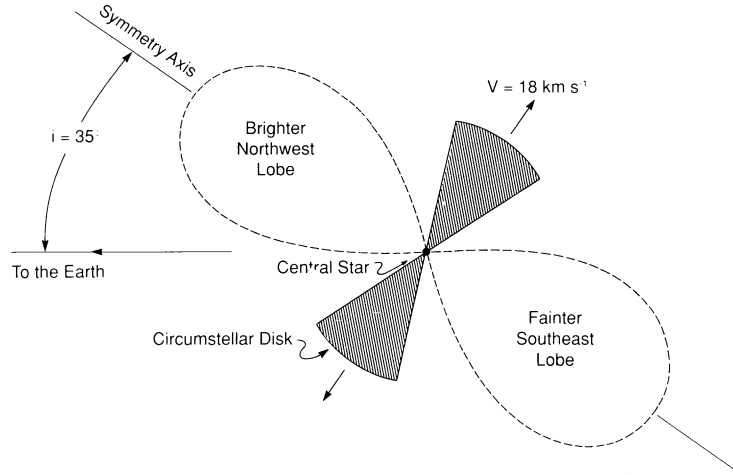


FIG. 4.—Schematic of the model used to produce Figs. 3(b), (d)

at constant speed  $V$  with a density distribution of the form

$$r = \begin{cases} \frac{A}{r^2} (\cos \theta)^N, & r \leq r_0, \\ 0, & r > r_0, \end{cases} \quad (1)$$

where  $r$  is the radial coordinate measured from the source of the outflow, and  $\theta$  is the latitude measured from the equatorial plane. This model describes a “fan-shaped” outflow with a FWHM width given by  $w = 2 \cos^{-1} [(\frac{1}{2})^{1/N}]$ . The disk is inclined to the line of sight such that the axis of the lobes makes an angle  $i$  with the line of sight. Figure 5 shows the geometry which relates the coordinates in the plane of the sky (unprimed) to the coordinates oriented with the midplane of the fan-shaped disk (primed). The equation yielding the brightness distribution across the disk is given by

$$I(x, y, V_z) = \int_{z_1}^{z_2} F(r, \theta) G(r, \theta) H(p, V_z, \phi) \rho(r, \theta) dz, \quad (2)$$

where  $p = (x^2 + y^2)^{1/2}$  and  $r = (p^2 + z^2)^{1/2}$ ,  $G(r, \theta)$  is a function

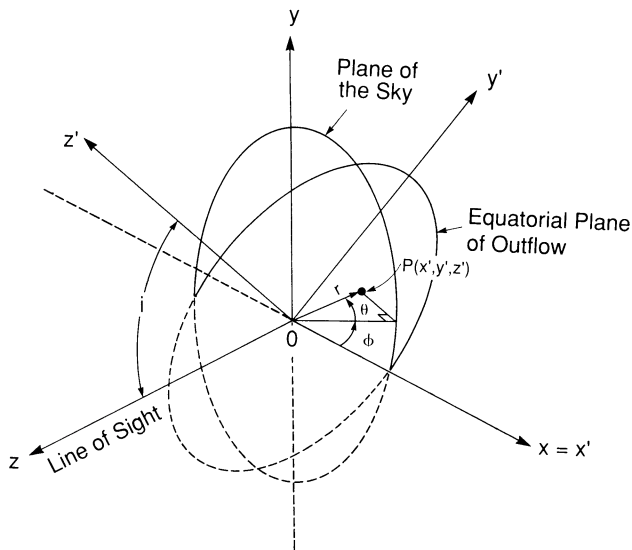


FIG. 5.—Diagram illustrating the relationship between coordinates in the plane of the sky and in the midplane of the circumstellar disk, used to model the 1667 MHz brightness and velocity distribution shown in Figures 3b and d.

which describes either the quenching of the pump due to collisions at high densities or the decline in OH abundance toward the star. We adopt  $G(r, \theta) = G_0 \{1 - \exp[-\alpha(r/r_0)^2 (\sec \theta)^N]\}$ , where  $\alpha$  is a constant and  $\theta$  is given by

$$\sin \theta = (y \sin i + z \cos i)/r. \quad (3)$$

Parameters  $z_1, z_2$  represent the range in  $z$  over which the radial velocity changes from  $V_z - \Delta V_z/2$  to  $V_z + \Delta V_z/2$ , where  $\Delta V_z$  is the velocity width produced by thermal or turbulent motions,  $F(r, \theta)$  is the volume pump rate due to IR photons,  $H(p, V_z, \phi)$  is the “competition factor” defined by Morris and Bowers (1980) describing the competition between streams of radiation in different directions at a given point, and  $\phi$  is the azimuthal angle between the line of nodes and the vector joining the central star to the line of sight.

Without a detailed knowledge of the pump mechanism, the dependence of the pump rate on position cannot be known. For simplicity, we have taken  $F(r, \theta)$  to be a constant. We have also assumed that  $H$  is constant since, as Morris and Bowers (1980) point out, it is roughly constant if the observer is located well out of the disk’s midplane. The simplifications are justified by the fact our model is largely illustrative, and not intended to derive rigorously the physical parameters of the system.

In the case when the thermal velocity width  $\Delta V_z$  is sufficiently small, the brightness distribution is given by

$$I(x, y, V_z) \propto \left\{ 1 - \exp \left[ -\alpha \frac{p^2 + z^2}{r_0^2} (\sec \theta)^N \right] \right\} \times \frac{A (\cos \theta)^N}{p^2 + z^2} \frac{p}{(1 - V_z^2/V^2)^{3/2}}, \quad (4)$$

where

$$z = (pV_z/V) [(1 - (V_z/V)^2)]^{-1/2}. \quad (5)$$

Intensities were computed numerically using equation (2) rather than equation (4) since the bin size or thermal width  $\Delta V_z$  was not necessarily small enough to justify using equation (4). A reasonable fit to the ZMM and FMM contours (Figs. 3b and d, respectively) is obtained by choosing  $i = 35^\circ$  (Davis, Seaquist, and Purton 1979),  $V = 18 \text{ km s}^{-1}$ ,  $N = 3.5$ ,  $r_0 = 2''.4$ ,  $\alpha = 0.4$ . The radius derived is in good agreement with the estimate made earlier from the ZMM in Figure 3a. The shape of

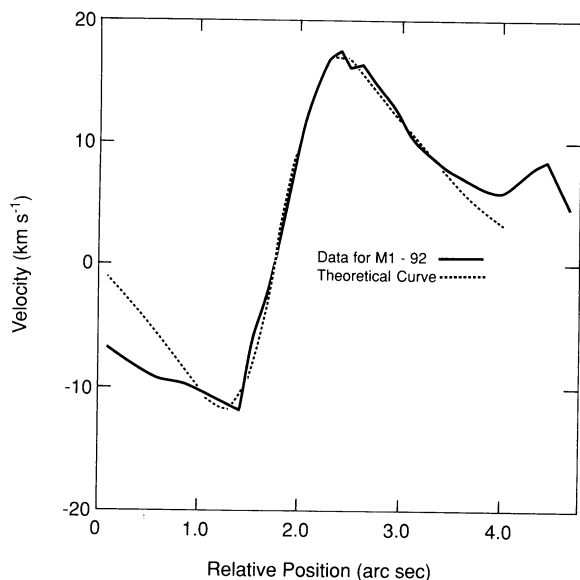


FIG. 6.—Observed and modeled first moment velocity profile along the axis of the bipolar lobes for  $i = 35^\circ$ ,  $N = 3.5$ , and  $\alpha = 0.4$ . The theoretical curve has been smoothed with a Gaussian corresponding to that of the “CLEAN beam.”

the velocity profile along the lobe axis is fairly sensitive to the value for  $N$ . The choice  $N = 3.5$  corresponds to  $w = 70^\circ$ . Figure 6 shows a comparison between the observed and theoretical velocity profiles at PA =  $131^\circ$  using these parameters. The model shows reasonable agreement with the main features of the OH emission and enables various features of the ZMM and FMM to be understood. For example, the outward decrease in mean radial velocity is produced by the increasing contribution toward the boundary of the envelope by gas away from the plane of the disk. At the point where the line of sight is tangent to the envelope boundary, the only gas observed is moving transverse to the line of sight. The model also accounts for the bright spots 2 and 4 as regions where the optical depth through the wind is greater, as shown in the model ZMM.

The model does not account, however, for either the apparent flattening of the velocity profile at the edge of the disk, or the occurrence of the hotspots 1 and 3 on the bipolar axis. The model ZMM does however show brightness maxima at the positions of peaks 1 and 3 in a slice profile measured along the projected bipolar axis. Note that Grinin (1985) developed a model of a bipolar nebula accounting for four brightness peaks produced by the effect of both radial expansion and rotation of the disk. Indeed, the predicted positions of the peaks are in agreement with those in M1–92. However, Figure 3c shows no evidence for rotation whatever. Note also that peaks 1 and 3 coincide with a region where the mean radial velocity is quite uniform in the plane of the sky. This effect would produce a concentration of beam-averaged emission at a particular velocity, but would not necessarily produce a peak in the integrated emission as observed in the ZMM. If, however, the velocities were aligned also along the line of sight, and if the maser were only partially saturated, then a peak in the ZMM could occur.

#### c) Mass-Loss Rate

In order to estimate the mass-loss rate, we follow an argument similar to that of Morris and Bowers (1980). The occurrence of a depression in the maser brightness near the position of the star is assumed to be produced by a quenching

of the maser by collisions between OH and  $H_2$  molecules where the density is high. A reasonable estimate of the radius where this occurs is about  $1''$ . If the maser emission is isotropic, then the volume emissivity of maser photons is  $(4\pi\Sigma I \Delta V_z)/(chL)$ , where  $I$  is the specific intensity at the above radius,  $c$  is the speed of light,  $h$  is Planck’s constant, and  $L$  is the path length. For a saturated maser this can be equated to the volume pump rate. From the ZMM in Figure 3c,  $\Sigma I \Delta V_z = 0.64 \text{ Jy (beam area)}^{-1} \text{ km s}^{-1}$ . We use for  $L$  the path corresponding to an angular distance of  $1''$  at 4.5 kpc ( $= 6.6 \times 10^{16} \text{ cm}$ ). The result is  $2.1 \times 10^{-8} \text{ photons s}^{-1} \text{ cm}^{-3}$ . Equating this pump rate to the collision rate for quenching of the maser as in Morris and Bowers (1980), we obtain

$$10^{-11}n(\text{OH})n(\text{H}_2) = 2.1 \times 10^{-8}, \quad (6)$$

and using  $n(\text{OH}) = 10^{-4}n(\text{H}_2)$ , we obtain  $N(\text{H}_2) = 5 \times 10^3 \text{ molecules cm}^{-3}$ . Since this density occurs at a radius of  $1''$  ( $6.6 \times 10^{16} \text{ cm}$  at 4.5 kpc), then  $A = 7.2 \times 10^{13} \text{ g cm}^{-1}$ . For the particular disk geometry adopted, the mass-loss rate in the disk is  $\dot{M} = 4\pi AV/(N+1)$ , where  $V = 18 \text{ km s}^{-1}$  and  $N = 3.5$ . Thus the mass-loss rate works out to  $5.6 \times 10^{-6} M_\odot \text{ yr}^{-1}$  in the disk for  $D = 4.5 \text{ kpc}$ . The estimate increases linearly with the assumed distance. This estimate is somewhat lower than that derived by Knapp (1986) from her CO measurements, although the difference is not at all inconsistent with the combined uncertainties in the input parameters assumed. In addition, our estimate refers only to the disk, whereas the CO estimate includes both the disk and the bipolar lobes.

#### d) M1–92 as a Young Planetary Nebula

We examine further characteristics of M1–92 which have a bearing on its presumed nature as a young planetary nebula.

With respect to its geometry and OH emission, about 50% of all PN exhibit bipolar geometry (Zuckerman and Aller 1986) and a number of young planetaries are known to possess OH emission (Zijlstra *et al.* 1989). In addition, the expansion velocities of the progenitor OH–IR star winds is in the range  $10\text{--}30 \text{ km s}^{-1}$ , which nicely brackets that of M1–92 ( $18 \text{ km s}^{-1}$ ). The systemic velocity of M1–92 ( $4 \text{ km s}^{-1}$ ) is rather low for a planetary, however, since generally their velocity dispersion is rather large ( $150 \text{ km s}^{-1}$ ).

We turn to the IR characteristics of M1–92. The IR colors from Table 1 are

$$\log [\lambda F_\lambda(25 \mu\text{m})/\lambda F_\lambda(12 \mu\text{m})] = 0.20 ;$$

$$\log [\lambda F_\lambda(60 \mu\text{m})/\lambda F_\lambda(25 \mu\text{m})] = -0.08 .$$

These fall in the range which is typical of late asymptotic giant branch (LAGB) stars in the color-color plot (Kwok 1989).

Furthermore, the data in Table 1 may be fitted to two black bodies (BB). The three longest wavelength *IRAS* data points fit a BB curve with  $T = 109 \text{ K}$ , which is in the range occupied by young PN. The short-wavelength IR emission fits a BB curve with  $T = 860 \text{ K}$  (Eiora, Hefele, and Zhong-Yu 1983). This is in the range occupied by Mira variables and OH–IR stars. Therefore, M1–92 exhibits IR emission with components characteristic of both preplanetary nebulae and young planetary nebulae.

The relationship between IR and 5 GHz radio emission in young PN has been discussed by Kwok, Hrivnak, and Milone (1986). Using their Figure 16, together with data from our Table 1 and the radio data from Bowers and Knapp (1986), we

find that for its far-IR flux, the 5 GHz flux is at the low end of the distribution for young PN, though not inconsistent with a young PN. As noted earlier, a comparison between the 5 GHz brightness distribution with Figure 3a shows that the peak radio brightness is displaced by 5".5 northwest from the minimum of the OH emission, approximately along the projected bipolar axis. The continuum peak is therefore well outside the OH boundary and spatially coincident with the northwestern bipolar lobe. Our 8.4 GHz high-resolution data show that this continuum peak is in fact an unresolved ( $<0.3$ ) source and leave open the question of whether it is physically associated with the lobe or simply a background source lying in the direction of the lobe. There is a tail of 5 GHz emission extending into the southeastern lobe, indicating that the radio continuum from this lobe appears to be much fainter. Our 8.4 GHz observations show no compact emission ( $<0.1$  mJy) within the OH emitting region, and therefore no emission associated with possible ionization at the inner edge of the disk.

The foregoing discussion suggests that M1-92 is indeed a young PN. The kinematic age of the system which can be estimated from its radius (2".4) and expansion velocity ( $18 \text{ km s}^{-1}$ ) is approximately 3000 ( $D/4.5 \text{ kpc}$ ) yr. Since this estimate exceeds that for the transition to a PN, which is 1500 yr (Schonberner 1983), there is no inconsistency with this conclusion.

#### V. CONCLUSIONS

The 1667 and 1612 MHz OH emission from the bipolar nebula M1-92 have been mapped in detail, and the results have yielded insight into the structure and kinematics of this bipolar nebula, and into the nature of this object itself.

The OH emission is found to originate in the disk which in the visual bisects the two lobes, and not in the lobes themselves. The main features of the OH emitting region are well explained by a simple axisymmetric model comprising a fan-

shaped disk expanding with a uniform velocity of  $18 \text{ km s}^{-1}$ . The disk has a radius of 2".4 ( $1.6 \times 10^{17} \text{ cm}$  if the distance is 4.5 kpc) and an opening angle (FWHM) of  $70^\circ$ . The OH is located in a toroidal region of this disk since there is an OH minimum at the center. The mass-loss rate in the disk is estimated to be about  $5.6 \times 10^{-6} M_\odot \text{ yr}^{-1}$ , based on an argument involving the quenching of the OH maser at high densities near the star and on an assumed distance of 4.5 kpc. The kinematic age of the disk is about 3000 yr.

The colors of the far-IR emission are characteristic of the LAGB phase, and the color temperature of 109 K is similar to that of young PN. A second blackbody may be fitted to the short-wavelength IR yielding 860 K, which is more characteristic of OH-IR stars and Mira variables. The radio continuum seen at 4.9 and 8.4 GHz appears to be associated predominantly with the northwestern lobe. The extended component may be thermal emission from gas in this lobe ionized by UV radiation escaping along the axis of the disk. However, the brightest feature is compact and may be an unrelated background source.

The optical and OH morphology, the IR and radio continuum characteristics, the kinematic age, and the inferred mass-loss rate associated with the disk, all taken together, suggest that M1-92 is a young planetary nebula. The central star is at the cool end of the temperature spectrum for a PN, however, which may be responsible for the rather weak continuum radio emission from this object. New maps of the radio thermal continuum morphology at higher resolution and sensitivity should now be made and compared in detail with the morphology of the optical lobes and the OH disk. Such a study should yield further insights into the temperature and luminosity of the central star and the nature of M1-92.

This research was supported by an operating grant to E. R. S. by the Natural Sciences and Engineering Research Council of Canada.

#### REFERENCES

- Abell, G. O. 1966, *Ap. J.*, **144**, 259.  
 Bowers, P. F., and Knapp, G. R. 1989, *Ap. J.*, **347**, 325.  
 Cohen, M., and Kuhl, L. V. 1977, *Ap. J.*, **213**, 79.  
 Davis, L. E., Seaquist, E. R., and Purton, C. R. 1979, *Ap. J.*, **230**, 434.  
 Eiroa, C., Hefele, H., and Zhong-Yu, Q. 1983, *Astr. Ap. Suppl.*, **54**, 309.  
 Elitzur, M. 1978, *Astr. Ap.*, **62**, 305.  
 Elitzur, M., Goldreich, P., and Scoville, N. 1976, *Ap. J.*, **205**, 384.  
 Fix, J. D., and Mutel, R. L. 1977, *Ap. Letters*, **19**, 37.  
 Grinin, V. P. 1985, *Izv. Krym. Astrofiz. Obs.*, **70**, 139.  
 Herbig, G. H. 1975, *Ap. J.*, **200**, 1.  
 Kaifu, N., et al. 1984, *Astr. Ap.*, **134**, 7.  
 Knapp, G. R. 1986, *Ap. J.*, **311**, 731.  
 Kwok, S. 1989, in *IAU Symposium 131, Planetary Nebulae*, ed. S. Torres-Peimbert (Dordrecht: Kluwer), p. 401.  
 Kwok, S., Hrivnak, B. J., and Milone, E. F. 1986, *Ap. J.*, **303**, 451.  
 Lada, C. J. 1985, *Ann. Rev. Astr. Ap.*, **23**, 267.  
 Leger, A., Klein, J., DeCheveigne, S., Guinet, C., Defourneau, D., and Belin, M. 1979, *Astr. Ap.*, **79**, 256.  
 Lepine, J. R. D., and Nguyen-Quang-Rieu 1974, *Astr. Ap.*, **36**, 469.  
 Minkowski, R. 1946, *Pub. A.S.P.*, **58**, 305.  
 Morris, M., and Bowers, P. F. 1980, *A.J.*, **85**, 724.  
 Morris, M., Bowers, P. F., and Turner, L. E. 1982, *Ap. J.*, **259**, 625.  
 Schonberner, D. 1983, *Ap. J.*, **272**, 708.  
 Takano, T., Fukui, Y., Ogawa, H., Takaba, H., Kawabe, R., Fujimoto, Y., Sugitani, K., and Fujimoto, M. 1984, *Ap. J. (Letters)*, **282**, L69.  
 Torrelles, S. M., Ho, P. T. P., Moran, J. M., Rodriguez, L. E., and Canto, J. 1986, *Ap. J.*, **307**, 77.  
 Zijlstra, A., Pottasch, S. R., te Lintel, P., and Bignell, C. 1989, in *IAU Symposium 131, Planetary Nebulae*, ed. S. Torres-Peimbert (Dordrecht: Kluwer), p. 210.  
 Zuckerman, B., and Aller, L. H. 1986, *Ap. J.*, **301**, 772.

L. E. DAVIS: Kitt Peak National Observatory, P.O. Box 26732, Tucson, AZ 85726

R. N. PLUME: Department of Astronomy, University of Texas, Austin, TX 78712

E. R. SEAQUIST: Department of Astronomy, University of Toronto, Toronto, Ontario, Canada M5S 1A7